VOLUME 30 NUMBER 3 July 2024
pISSN 2287-2728
eISSN 2387-285X

CLINICAL and MOLECULAR HEPATOLOGY

The forum for latest knowledge of hepatobiliary diseases

Spears and shields for liver transplantation

Sorafenib versus Lenvatinib Post-ATE/BEV in HCC
Bariatric intervention improves MASH
Non-liver cancer risk of ETV vs TDF
Dynamic changes in MASLD and HCC risk

KASL

pISSN 2287-2728
eISSN 2287-285X

CLINICAL and MOLECULAR HEPATOLOGY

https://doi.org/10.3350/cmh.2024.0047
Clinical and Molecular Hepatology 2024;30:449-467

Original Article

Ursolic acid targets secreted phosphoprotein 1 to regulate Th17 cells against metabolic dysfunction-associated steatotic liver disease

Yiyuan Zheng[1,*], Lina Zhao[2,3,*], Zhekun Xiong[4,*], Chaoyuan Huang[5,6], Qiuhong Yong[3,7], Dan Fang[8], Yugang Fu[1], Simin Gu[1], Chong Chen[1], Jiacheng Li[1], Yingying Zhu[1], Jing Liu[1], Fengbin Liu[2,3], and Yong Li[1]

[1]Department of Gastroenterology, Shanghai Municipal Hospital of Traditional Chinese Medicine, Shanghai University of Traditional Chinese Medicine, Shanghai, China; [2]Department of Gastroenterology, The First Affiliated Hospital of Guangzhou University of Chinese Medicine, Guangzhou, China; [3]Lingnan Medical Research Center, Guangzhou University of Chinese Medicine, Guangzhou, China; [4]Department of Spleen, Stomach and Hepatobiliary, Zhongshan Hospital of Traditional Chinese Medicine, Zhongshan, China; [5]Department of Gastroenterology, The Second Affiliated Hospital of Guangzhou University of Chinese Medicine, Guangzhou, China; [6]Department of Gastroenterology, Guangdong Provincial Hospital of Chinese Medicine, Guangzhou, China; [7]The First Clinical Medical School, Guangzhou University of Chinese Medicine, Guangzhou, China; [8]Medical Affairs Department, Ton-Bridge Medical Technology Co., Ltd., Zhuhai, China

Graphical Abstract

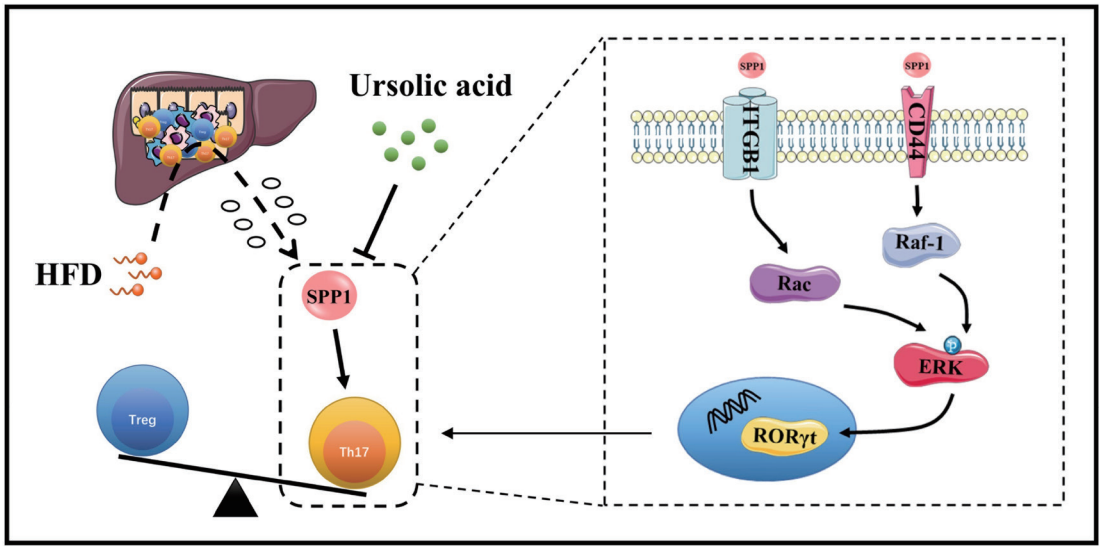

Study Highlights

- Ursolic acid can directly bind with SPP1 to regulate its activity.
- SPP1 promotes Th17 cell differentiation via interactions with ITGB1 and CD44.
- Ursolic acid ameliorates immune inflammation in MASLD by modulating SPP1-mediated Th17 cell differentiation.

Background/Aims: Metabolic dysfunction-associated steatotic liver disease (MASLD) has become an increasingly important health challenge, with a substantial rise linked to changing lifestyles and global obesity. Ursolic acid, a natural pentacyclic triterpenoid, has been explored for its potential therapeutic effects. Given its multifunctional bioactive properties, this research further revealed the pharmacological mechanisms of ursolic acid on MASLD.

Methods: Drug target chips and bioinformatics analysis were combined in this study to explore the potential therapeutic effects of ursolic acid on MASLD. Molecular docking simulations, surface plasmon resonance analyses, pull-down experiments, and co-immunoprecipitation assays were used to verify the direct interactions. Gene knockdown mice were generated, and high-fat diets were used to validate drug efficacy. Furthermore, initial $CD4^+$ T cells were isolated and stimulated to demonstrate our findings.

Results: In this study, the multifunctional extracellular matrix phosphorylated glycoprotein secreted phosphoprotein 1 (SPP1) was investigated, highlighting its capability to induce Th17 cell differentiation, amplifying inflammatory cascades, and subsequently promoting the evolution of MASLD. In addition, this study revealed that in addition to the canonical TGF-β/IL-6 cytokine pathway, SPP1 can directly interact with ITGB1 and CD44, orchestrating Th17 cell differentiation via their joint downstream ERK signaling pathway. Remarkably, ursolic acid intervention notably suppressed the protein activity of SPP1, suggesting a promising avenue for ameliorating the immunoinflammatory trajectory in MASLD progression.

Conclusions: Ursolic acid could improve immune inflammation in MASLD by modulating SPP1-mediated Th17 cell differentiation via the ERK signaling pathway, which is orchestrated jointly by ITGB1 and CD44, emerging as a linchpin in this molecular cascade. **(Clin Mol Hepatol 2024;30:449-467)**

Keywords: Metabolic dysfunction-associated steatotic liver disease; Ursolic acid; Secreted phosphoprotein 1; Th17 cells

INTRODUCTION

Metabolic dysfunction-associated steatotic liver disease (MASLD) is typified as a multi-systemic metabolic stress-induced hepatic derangement, with its spectrum encompassing simple steatosis, metabolic dysfunction-associated

Corresponding author : **Yong Li**
Shanghai Municipal Hospital of Traditional Chinese Medicine, Shanghai University of Traditional Chinese Medicine, 274 Zhijiang Middle Road, Shanghai 200071, China
Tel: +86-021-56639828, Fax: +86-021-56639828, E-mail: liyong@shutcm.edu.cn
https://orcid.org/0009-0001-3141-8114

Fengbin Liu
The First Affiliated Hospital of Guangzhou University of Chinese Medicine, 16 Airport Road, Guangzhou 510405, Guangdong, China
Tel: +86-020-36591912, Fax: +86-020-36591912, E-mail: liufengbin163@163.com
https://orcid.org/0000-0002-8957-9260

*These authors contributed equally to this work.

Editor: Sungsoon Fang, Yonsei University College of Medicine, Korea

Received : Jan. 18, 2024 / **Revised :** Apr. 12, 2024 / **Accepted :** Apr. 15, 2024

Abbreviations:

MASH, metabolic dysfunction-associated steatohepatitis; SPP1, secreted phosphoprotein 1; ITGB1, integrin β1; ECM, extracellular matrix; HSCs, hepatic stellate cells; ERK, extracellular signal-regulated kinase; HFD, high-fat diets; NCD, normal control diets; ALT, alanine aminotransferase; AST, aspartate aminotransferase; IPGTT, intraperitoneal glucose tolerance tests; ITT, insulin tolerance tests; NAS, MASLD activity score; DEGs, differentially expressed genes; ROC, receiver operating characteristic; AUC, area under the curve; SPR, surface plasmon resonance; KD, knockdown; AAV, adeno-associated virus; WT, wild-type; CD44A, CD44 antagonists; MAFLD, metabolic dysfunction-associated fatty liver disease; MASLD, metabolic dysfunction-associated steatotic liver disease

https://doi.org/10.3350/cmh.2024.0047

steatohepatitis (MASH), and concomitant hepatic fibrosis and cirrhosis, culminating in the potential development of hepatocellular carcinoma.[1] With global obesity trends driven by evolving lifestyles, the incidence of MASLD has been steadily increasing over the past decades. Epidemiological surveys indicate a staggering global prevalence of MASLD approaching 25%, with an estimated 20% having the propensity to evolve into MASH, posing significant health risks and substantial economic burdens on society.[2,3] Most notably, a cohort study underscores that even mild steatosis can markedly augment all-cause mortality risk, which is also tightly correlated with disease severity.[4] Contrasted against this dire backdrop, existing therapeutic approaches for MASLD have been underwhelming, amplifying the urgency for innovative drug exploration.[5,6]

Ursolic acid, a pentacyclic triterpenoid naturally ubiquitously distributed amongst diverse plant species, is rendered particularly noteworthy owing to its intrinsic chemical structure bestowing upon it a gamut of unique bioactivities, including anti-inflammatory, anti-oxidative and anti-tumour properties.[7] In recent years, this natural triterpenoid has manifested exceptional potential in drug development for a plethora of ailments, and researches have spotlighted its multifarious roles in lipid regulation, inflammatory and oxidative damage mitigation, as well as in gut microbiota modulation, collectively offering a bulwark against MASLD.[8,9] Nonetheless, considering its multifunctional bioactive properties, unveiling the definitive pharmacological mechanisms of ursolic acid on MASLD remains paramount.

While the precise pathogenesis of MASLD is still not fully elucidated, current researches emphasize the intricate interplay of metabolic stress, immune inflammation, hypoxic injury, insulin resistance and gut microbiota dysbiosis.[10] Of note, the dynamic equilibrium in hepatic immune homeostasis between helper T (Th) 17 cells and regulatory T (Treg) cells emerges as a cardinal nexus mediating immune stress and inflammatory responses, hence garnering widespread scrutiny.[11,12] Particularly, Th17 cells, a subtype of $CD4^+$ T-helper cells, can evolve under stimuli like transforming growth factor (TGF)-β and interleukin (IL)-6, subsequently secreting IL-17 and other critical inflammatory cytokines, thereby amplifying inflammatory cascades, and further galvanizing stellate cell activation and fibrogenesis.[13-15] Given that cutting-edge discoveries accentuate the centrality of secretory factor-mediated intercellular crosstalk in metabolic inflammatory responses, this present investigation directs its focus towards secreted phosphoprotein 1 (SPP1), alternatively known as osteopontin, through the integration of bioinformatics analyses and drug target chip assays.[16,17]

As a crucial component of the extracellular matrix (ECM), SPP1 is a multifunctional phosphorylated glycoprotein, secreted by a myriad of cells, including bone marrow cells, activated T cells, macrophages, endothelial cells, parenchymal cells, etc.[18] With numerous phosphorylation and glycosylation motifs, SPP1 partakes in modulating cell adhesion and migration, immune inflammation and tissue remodelling, holding a position of significant importance within the hepatic microenvironment.[19] The latest studies demonstrate that SPP1 is able to induce the differentiation of Th17 cells while inhibiting their apoptosis to maintain an immune-inflammatory state, subsequently facilitating the activation of hepatic stellate cells (HSCs) and promoting the progression from MASLD to MASH and liver fibrosis.[20] Intriguingly, this current investigation discerns that apart from the canonical TGF-β/IL-6 cytokine pathway, SPP1 can also directly bind to the cell surface receptors, integrin β1 (ITGB1) and CD44, inducing the differentiation of Th17 cells by modulating their joint downstream extracellular signal-regulated kinase (ERK) signaling pathway. Moreover, the therapeutic intervention with ursolic acid suppresses the protein activity of SPP1, thereby ameliorating the immunoinflammatory state during MASLD progression.

MATERIALS AND METHODS

Bioinformatic analysis

Expression profiles pertinent to nonalcoholic fatty liver disease (NAFLD) and nonalcoholic steatohepatitis (NASH) were systematically retrieved from the Gene Expression Omnibus (GEO) database, utilizing the search parameters: (“fatty liver”[MeSH Terms] OR fatty liver[All Fields] OR NAFLD[All Fields] OR NASH[All Fields]) AND “Homo sapiens”[porgn]. Exclusion criteria encompassed datasets deemed as having irrelevant data, an absence of controls, or a predominance of post-operative subjects. Following a stringent review, two microarrays, GSE49541 and

GSE89632, were meticulously selected, which notably delineated the intricate comparative stages between NAFLD and NASH. To ensure coherency and mitigate potential variances arising from differing experimental conditions or platforms, batch normalization was judiciously executed on all integrated microarray datasets using the limma package in R version 4.0 (R Foundation, Vienna, Austria). The integrated datasets were subsequently processed to discern differentially expressed genes, and those with adjusted *P*-values below 0.05 were designated as statistically significant.

To acquire a holistic understanding of the biological functions and pathways associated with the identified differentially expressed genes, enrichment analysis was performed. Leveraging the Bioconductor packages, specifically org.Hs.eg.db and clusterProfiler, key pathways and functional categories were elucidated. A comprehensive protein-protein interaction network was meticulously constructed using the Search Tool for the Retrieval of Interacting Genes (STRING) database. This protein-protein interaction (PPI) network served as an invaluable framework, providing insights into the functional relationships between identified proteins, while centrality analysis, pivotal for discerning nodes of paramount importance within the network, was systematically executed based on the intricate interaction relationships between nodes.

Drug-targets interaction analysis

An extensive probe into the interactions between ursolic acid and potential protein targets was carried out utilizing the HuProt™20K human proteomics microarray. Ursolic acid was conjugated with biotin, generating a bio-ursolic acid probe complex. In strict adherence to the protocols delineated by Wayen Biotechnologies Co. Ltd., the chip was hybridized with both bio-ursolic acid and its biotin control. Ensuing incubation, the chip underwent analysis with a GenePix 4000B microarray scanner (Axon Instruments, Foster City, CA, USA), and subsequent data interpretation was executed employing GenePix Pro v6.0.

The interactions between ursolic acid and specific binding proteins were verified by Surface Plasmon Resonance technology using a biacore sensor chip (28980887; Univbio, Shanghai, China). Target proteins were diluted and coupled under fixed time conditions, with ethanolamine addressing any unbound activation groups. Subsequently, varying concentrations of bio-ursolic acid were introduced, employing a running buffer as control. Parameters included a flow rate of 30 μL/min, along with binding and dissociation phases of 90 s and 120 s, respectively. Data acquisition followed a multi-cycle approach, and post double reference deduction, data extrapolation was conducted using the Biacore T200 analysis software (Cytiva, Marlborough, MA, USA).

Molecular docking simulations were executed to predict the preferential binding orientations and affinities of ligands within the active site of a target protein. The three-dimensional structure of the protein target was sourced from the Protein Data Bank and processed to remove water molecules, add missing hydrogens, and optimize the protonation states of amino acid residues. Using the AutoDock Vina software (Scripps Research, La Jolla, CA, USA) suite, grid boxes were set up around the active site with dimensions tailored to encompass key residues and potential ligand binding sub-sites. The ligands were prepared by assigning Gasteiger charges, generating 3D conformations, and optimizing their geometries. The docking procedure was executed employing the Lamarckian Genetic Algorithm, and the generated docking poses were ranked based on the Vina scoring function. To account for flexibility, the side chains of the residues within a defined radius of the active site were set as flexible. The top-ranked poses, determined by binding energy scores, were visualized and analysed in PyMOL (DeLano Scientific, San Carlos, CA, USA) and further subjected to post-docking validation using molecular dynamics simulations to ensure the stability and feasibility of the predicted complexes.

Animal model

Six-week-old male C57BL/6J mice were obtained from the Medical Experimental Animal Center of Guangdong Province. Pursuant to rigorous ethical considerations, all animal experiments were conducted in strict accordance with project licenses (TCMF1-2021001 and TCMF1-2022052), which received the endorsement of the Institutional Animal Care and Use Committee of Guangzhou University of Chinese Medicine. Furthermore, all procedures adhered faithfully to the ARRIVE guidelines to ensure the humane treatment of the animals.

https://doi.org/10.3350/cmh.2024.0047

All animals were housed under standard environment and had access to food and water ad libitum. After one-week acclimatization, these mice were randomized equally into different groups, and were reared under a controlled condition. These mice were fed with high-fat diets (D12492; Research Diets, New Brunswick, NJ, USA) as well as normal control diets (NCD, D12450J, Research Diets) for 12 weeks to construct MASLD mice model, and ursolic acid (U820363, Macklin, Shanghai, China) was given to the treatment group by oral gavage at doses of 25, 50, and 100 mg/kg/d as intervention therapy, while normal saline was administered daily to the HFD and control groups.

Recombinant adeno-associated virus serotype 8 (AAV2/8) vectors were employed for in vivo gene delivery. Specifically, AAV2/8 harboring a CMV-driven shRNA targeting SPP1 (sequence: 5'-GATGACTTTAAGCAAGAAA-3') and the control AAV2/8-CMV-Null were obtained from Obio Technology Co. Ltd., AAV vectors were propagated in HEK293T cells, purified, and then concentrated to achieve a final titer of approximately 1×10^{13} genome copies per millilitre. Adult male C57BL/6 mice, aged between 8–10 weeks, were acclimated and then randomly assigned to either the AAV2/8-shSPP1 or AAV2/8-Null groups. For delivery, 100 μL of the respective virus preparation was intraperitoneally injected into each mouse. Following the injection, mice were closely monitored, and tissue collection for assessment of AAV-mediated gene knockdown was typically conducted 4 weeks post-injection, a time frame optimized for peak AAV-mediated transgene expression in the liver.

A systematic documentation approach was implemented, wherein body weights of the subjects were recorded on a weekly basis. Upon the culmination of the experiment, liver weights were accurately determined. Extracted liver samples were either immediately snap-frozen in liquid nitrogen or fixed in 4% paraformaldehyde (PFA, BL539A; Biosharp, Beijing, China), earmarked for subsequent analyses.

Cell culture

Mice were euthanized in accordance with institutional and ARRIVE guidelines. Spleens were aseptically harvested from euthanized C57BL/6J mice. Following mechanical disruption, single-cell suspensions were obtained by passing the tissue through a 70 μm cell strainer (258368; NEST, Wuxi, China). Red blood cells were lysed using ACK lysing buffer (A1049201; Invitrogen, Waltham, MA, USA), and the splenocytes were washed twice with phosphate buffered saline (PBS, BL302A; Biosharp). $CD4^+$ T cells were isolated using magnetic-activated cell sorting with a Mouse $CD4^+$ T cell Isolation Kit (130-104-454; Miltenyi, Auburn, CA, USA), as per the manufacturer's guidelines. Subsequently, for Th17 cell differentiation, naive $CD4^+$ T cells were cultured in RPMI 1640 medium (C11875500BT; Invitrogen) supplemented with 10% fetal bovine serum (FBS, 10091-148; Invitrogen), 1% penicillin-streptomycin (15140-122; Invitrogen), and activated with plate-bound anti-CD3 (2 μg/mL) and anti-CD28 (1 μg/mL) antibodies (11453D; eBioscience, Carlsbad, CA, USA). The culture medium was supplemented with IL-6 (20 ng/mL, AF-216-16-50; PeproTech, Rocky Hill, NJ, USA), TGF-β (3 ng/mL, RP02523; ABclonal, Wuhan, China), anti-IFN-γ (2 μg/mL, 16-7311-85; eBioscience) and anti-IL-4 (2 μg/mL, 14-7041-85; eBioscience) to promote Th17 differentiation.

Upon initiating Th17 polarization, the cells were concurrently treated with various concentrations of recombinant SPP1 protein (RP02806; ABclonal) and ursolic acid. To assess the influence of ITGB1 and CD44 modulation on Th17 differentiation, cells were additionally co-incubated with ITGB1 inhibitor GLPG0187 (1 nM, HY-100506; MedChemExpress, Monmouth, NJ, USA) or CD44 antagonist (1 μg/mL, 553131; BD Biosciences, San Jose, CA, USA) at specific concentrations recommended by preliminary dose-response studies. After a 72-hour incubation at 37°C in a 5% CO_2 humidified atmosphere, cells were harvested for further assays. Finally, Th17 cell differentiation efficiency was evaluated by intracellular staining of IL-17A followed by flow cytometry analyses.

IPGTT and ITT

During the last week of the experiment, mice were fasted for 6 hours with water provided ad libitum. Prior to glucose administration, a baseline blood sample was obtained via tail vein nick for the determination of fasting blood glucose levels. Mice were then intraperitoneally injected with a solution of glucose (2 g/kg body weight, G8270; Sigma, St. Louis, MO, USA) dissolved in sterile saline. Blood glucose measurements were taken at intervals of 15, 30, 60, 90, and 120 minutes post-injection to monitor the glucose

clearance rate. After a one-day adaption, following a 4-hour fasting period, mice received intraperitoneal injections of insulin (0.75 IU/kg body weight, 91077C; Sigma), and the glucose levels were determined as described above.

Quantitative real-time polymerase chain reaction (qRT-PCR)

Liver tissues were carefully dissected and immediately immersed in TRIzol reagent (15596026; Invitrogen) for RNA extraction, in accordance with the manufacturer's instructions, while the concentrations were determined using a NanoDrop 2000c spectrophotometer (Thermo Fisher Scientific, Sunnyvale, CA, USA), with A260/A280 ratios between 1.8 and 2.0 considered acceptable for subsequent applications. Complementary DNA (cDNA) was synthesized using the PrimeScript RT Reagent Kit (RR036A; Takara, Shiga, Japan), while TB Green Premix Ex Taq II (RR420A; Takara) was used to conduct qRT-PCR based on Bio-Rad CFX96 Real-Time PCR System (Hercules, CA, USA). Thermal cycling conditions encompassed an initial denaturation phase at 95°C for 30 s, followed by 40 amplification cycles at 95°C for 5 s and 60°C for 30 s. The relative mRNA levels of target genes were calculated by $2^{-\Delta\Delta Ct}$, and beta-actin was used to normalize the samples. All primer sequences used in this study are listed in Supplementary Table 1.

Western blotting

Liver tissues were meticulously dissected and homogenized in RIPA lysis buffer (P0013B; Beyotime, Shanghai, China) supplemented with protease and phosphatase inhibitors (P1045; Beyotime) to ensure the retention of protein integrity. The homogenates were centrifuged at 14,000 × g for 15 minutes at 4°C. Supernatants were harvested, and the protein concentrations were determined using a BCA protein assay kit (P0010; Beyotime). Equal amounts of protein from each sample were mixed with loading buffer and boiled for 5 minutes to denature. The samples were then subjected to sodium dodecyl sulfate-polyacrylamide gel electrophoresis (SDS-PAGE) on gels with appropriate concentrations, depending on the molecular weight of the target protein. Separated proteins in the gel were transferred onto polyvinylidene fluoride (PVDF) membranes (ISEQ00010; Millipore, Billerica, MA, USA) using a wet transfer system. The membranes were blocked in 5% milk (232100; BD Biosciences) dissolved in Tris-buffered saline containing 0.1% Tween-20 (ST825; Beyotime) for 1 hour at room temperature to prevent non-specific binding. The membranes were then incubated with primary antibodies specific to the target proteins overnight at 4°C. Following primary antibody incubation, the membranes were washed thrice with TBST and then incubated with corresponding secondary antibodies for 1 hour at room temperature. Following another series of washes, the bound antibodies were visualized using an enhanced chemiluminescence (ECL, 1705060; Bio-Rad) detection system. Images were captured by a ChemiDoc XRS System (Bio-Rad), and the intensity of the bands was quantified using ImageJ 1.8.0 (National Institutes of Health, Bethesda, MD, USA). To ensure accurate quantification, β-actin was used as an internal control.

Primary antibodies against ITGB1 (1:2,000, 34971), ITGB3 (1:2,000, 13166), p-ERK (1:2,000, 4370), ERK (1:2,000, 4695) and β-actin (1:2,000, 4970) were obtained from Cell Signaling Technology, against CD44 (1:1,000, ab189524) were purchased from Abcam, and against SPP1 (1:2,000, sc-21742) were purchased from Santa Cruz Biotechnology.

Histological staining

Liver specimens from the murine cohort underwent two distinct histological procedures for optimal morphological evaluation. Frozen liver sections were air-dried and fixed in 10% neutral buffered formalin (RL3223; Bioroyee, Beijing, China). Following fixation, sections underwent Oil Red O (C0157S; Beyotime) staining to visualize lipid droplets. Afterward, sections were rinsed and counterstained with Mayer's hematoxylin and subsequently mounted with an aqueous mounting medium. Finally, images were observed on an Olympus BX-50 microscope (Tokyo, Japan), and for quantification of lipid accumulation, the percentage of the Oil Red O-positive area to the total area was calculated using ImageJ software.

Liver sections from paraffin blocks were deparaffinized, rehydrated, and stained with hematoxylin and eosin (H&E, G1005; Servicebio, Wuhan, China) referring to the stand-

https://doi.org/10.3350/cmh.2024.0047

ard procedure. Following staining, the MASLD activity score was measured to assess the severity of steatosis (graded 0-3 based on the percentage of hepatocytes containing fat), lobular inflammation (graded 0-3 based on the number of inflammatory foci), and hepatocellular ballooning (graded 0-2). Thus, the cumulative score provided an overall assessment of liver pathology.

An immunohistochemistry kit (G1215; Servicebio) was applied in this research. According to the relevant protocols, liver tissues were cut into 4 μm sections from the paraffin blocks. Deparaffinized and hydrated were conducted, and sodium citrate solution was used for antigen retrieval. Liver sections were immune-stained with antibodies against SPP1 (1:50), ROR gamma (1:100, abs124841; Absin, Shanghai, China), or IL-17A (1:100, ab79056; Abcam, Cambridge, UK), and the colour reaction was developed using biotinylated immunoglobin G, horseradish peroxidase-streptavidin and diaminobenzidine. Finally, images were observed on an Olympus BX-50 microscope, and the positive staining area and intensity for each marker were quantified using ImageJ software, which was calibrated against control sections.

Flow cytometry

Liver tissues from mice were harvested and immediately frozen in liquid nitrogen to preserve cell integrity. These frozen tissues were then mechanically disrupted using a mortar and pestle under liquid nitrogen conditions, ensuring the tissues were kept thoroughly frozen throughout the process to minimize cell damage. The powdered liver tissue was then gently resuspended in a cold PBS buffer supplemented with 2% FBS to generate a single-cell suspension. Following thawing, the single-cell suspensions were filtered through a 70 μm cell strainer to eliminate large tissue debris and to obtain a cleaner cell population.

Before proceeding to stain, cells were resuspended in an RPMI 1640 medium and stimulated with phorbol myristate acetate and ionomycin (110007; Prosperch, China) in the presence of brefeldin A (110008; Prosperch) for 6 hours at 37°C in a 5 % CO_2 atmosphere. This stimulation step ensured that cytokines, especially IL-17A, were retained inside the cells, allowing for intracellular staining. Subsequently, cells were blocked with anti-mouse CD16/CD32 (Fc Block, 553141; BD Biosciences) for 15 minutes at 4°C to minimize nonspecific antibody binding. Subsequently, cells were stained with fluorescence-conjugated antibodies against CD3 (HT1610025; Otwo, Shenzhen, China) and CD4 (HT1610043; Otwo) for 30 minutes in the dark at 4°C. For intracellular staining of IL-17A, cells previously stained with surface markers were fixed and permeabilized using the Cytofix/Cytoperm Fixation and Permeabilization Solution (554714; BD Biosciences). Post-permeabilization, cells were stained with a fluorescence-conjugated antibody against IL-17A (HT1610485; Otwo) for 30 minutes in the dark at 4°C. The stained cells were then washed and resuspended in the staining buffer, after which they were subjected to flow cytometric analysis. Finally, data acquisition was conducted on NovoCyte D2060R (Agilent, Palo Alto, CA, USA), and the analyses were performed by FlowJo v10.8 (BD Biosciences).

Pull-down assay

The Desthiobiotinylation and Pull-Down Kit (P0637S; Beyotime) was used in this study for the co-immunoprecipitation assay. Ursolic acid-conjugated agarose beads were prepared by covalently linking ursolic acid to activated agarose beads using the manufacturer's protocol. Unreacted sites on the beads were blocked using a quenching agent, and the beads were washed thoroughly to remove any unbound ursolic acid. Fresh liver tissues were homogenized in a lysis buffer enriched with protease and phosphatase inhibitors. Gentle mechanical homogenization was implemented to ensure optimal tissue disruption. The homogenates were centrifuged at 12,000 × g for 10 minutes at 4°C, and the clarified supernatants were collected. The ursolic acid-conjugated agarose beads were added to the liver lysates and incubated overnight at 4°C on a rotating platform; this allowed for the specific binding of SPP1 or other potential interacting proteins to ursolic acid. After incubation, the beads were pelleted by brief centrifugation. The cells were then washed multiple times with lysis buffer to remove non-specifically adhered proteins. For protein elution, beads were resuspended in Laemmli buffer and boiled for 5 minutes. Eluted proteins were then separated using SDS-PAGE and transferred onto PVDF membranes for Western blotting.

Co-immunoprecipitation assay

The rProtein A/G Magnetic IP/Co-IP Kit (abs9649; Absin) was employed for the co-immunoprecipitation assay. Liver tissues and Th17 cells were initially lysed in a RIPA buffer supplemented with protease and phosphatase inhibitors to ensure the preservation of protein integrity. Tissue disruption was facilitated using gentle mechanical homogenization, ensuring uniform lysis. The resultant lysates were centrifuged at 12,000 × g for 10 minutes at 4°C, and the supernatants were collected for subsequent procedures. For pre-clearing, each supernatant was incubated with protein A/G PLUS-agarose beads for 1 hour at 4°C on a rotator. Post-incubation, the samples were centrifuged to pellet the agarose beads, and the pre-cleared supernatants were collected. SPP1-specific antibody (1 μg per 100 μg of total protein) was added to the pre-cleared lysates, followed by overnight incubation at 4°C on a rotating platform to enable the formation of immunocomplexes. Post-overnight incubation, protein A/G PLUS-agarose beads were added to the lysate-antibody mixture, followed by a further 2-hour incubation at 4°C. The agarose beads, now bound to the immunocomplexes, were subsequently pelleted through centrifugation. The pelleted beads were washed thrice with the RIPA buffer to remove non-specifically bound proteins. After the final wash, the beads were resuspended in Laemmli buffer and boiled for 5 minutes to elute the immunocomplexed proteins. Finally, SDS-PAGE and Western blotting procedures were employed to detect the presence of ITGB1, ITGB3, and CD44 in the eluted protein complexes.

Statistical analysis

All quantitative data generated during this study were collated and represented as mean ± standard error of the mean. The GraphPad Prism 7.0 software suite (GraphPad Software, San Diego, CA, USA) was enlisted for the entirety of our data visualization and subsequent statistical computations. One-way analysis of variance was conducted for data analyses among groups, and *P*-value <0.05 was considered statistically significant.

RESULTS

Ursolic acid exerts multifaceted therapeutic effects on MASLD

Our previous studies have demonstrated that ursolic acid has the capability to modulate the protein activity of decorin, subsequently regulating the IGF-IR and HIF-1 signaling pathways, thereby furnishing a dual protective effect against metabolic dysfunction and hepatic hypoxia during the progression of MASLD.[21] Nevertheless, given the multifunctional biological activities associated with ursolic acid, we are inclined to further delve into its myriad pharmacological mechanisms. In this experimental research, the therapeutic efficacy of ursolic acid against MASLD-induced metabolic stress and immune inflammation was revalidated using a high-fat diet (HFD) mouse model. The results illustrated that intervention treatment with ursolic acid effectively alleviated weight gain induced by the high-fat diet in a dose-dependent manner, with statistically significant differences in weight emerging from the sixth week between the model and high-dose treatment groups and from the eighth and tenth weeks with the medium- and low-dose treatment groups, respectively (Fig. 1A). By the termination of this experiment at the twelfth week, liver weight measurements exhibited a notable reduction in both liver weight and liver index, calculated by the ratio of liver to body weight, following ursolic acid intervention (Fig. 1B); concurrently, evaluations on both serum and hepatic lipid concentrations underscored its role in improving lipid metabolism (Fig. 1C). Additionally, serum alanine aminotransferase and aspartate aminotransferase assays depicted a significant improvement in liver dysfunction, highlighting the feasibility of employing ursolic acid in the treatment of MASLD. Intraperitoneal glucose tolerance tests (IPGTT) and insulin tolerance tests (ITT) confirmed that the high-fat diet compromised glucose tolerance and precipitated insulin resistance in mice, both of which were critical pathological foundations for MASLD, while the intervention treatment of ursolic acid rendered protection against these perturbations (Fig. 1D and Supplementary Fig. 1A). Histopathological staining of liver tissues demonstrated pronounced lipid droplet accumulation, formation of fatty vacuoles and inflammatory cell infiltration in mice subjected to the high-fat diet, and intervention with ursolic acid could offer therapeutic effects

https://doi.org/10.3350/cmh.2024.0047

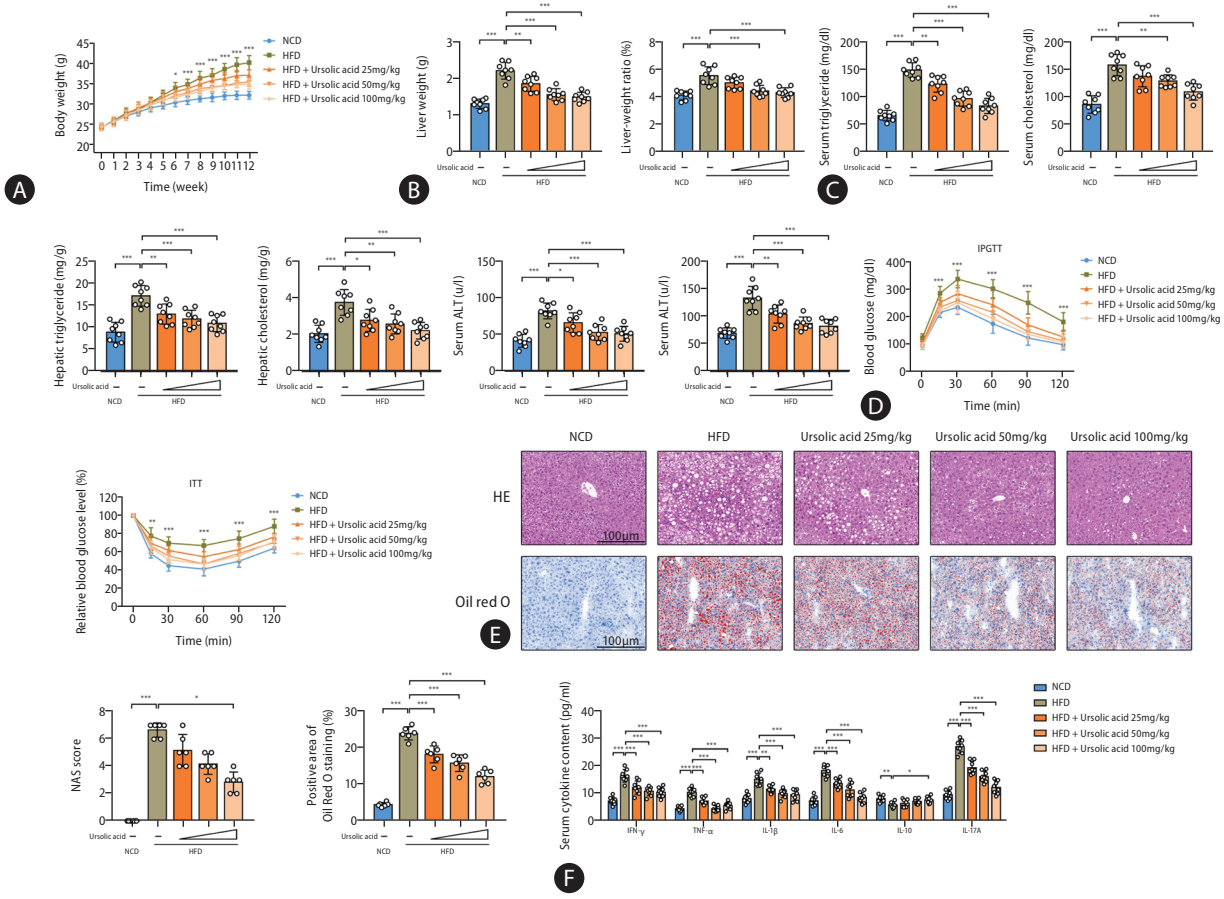

Figure 1. Ursolic acid exerts multifaceted therapeutic effects on MASLD. (A) Body weights were recorded weekly. (B) Liver weights were measured by the termination of this experiment at the twelfth week, and liver indexes were calculated by the ratio of liver to body weight. (C) Serum and hepatic lipid concentrations were determined by an automatic biochemical analyzer. (D) IPGTT and ITT were performed to monitor glucose tolerance and insulin resistance. (E) Histological staining of H&E and oil red O in liver tissues was used to observe the inflammatory cytokine infiltration and lipid droplet accumulation. The MASLD activity scores were computed by steatosis, intralobular inflammation, and hepatocyte ballooning to assess disease severity. The positive area of Oil red O staining was estimated for quantification of lipid accumulation. (F) Serum inflammatory cytokines were detected to detect inflammatory reactions. MASLD, metabolic dysfunction-associated steatotic liver disease; IPGTT, intraperitoneal glucose tolerance tests; ITT, insulin tolerance tests; SD, standard deviation; HFD, high-fat diets; NCD, normal control diets. Data are represented as mean±SD. n=6-8. **P*<0.05, ***P*<0.01, ****P*<0.001.

against all of these conditions, with the MASLD activity score, an indicator to assess the progression of MASLD, showcasing the most significant therapeutic effects in the high-dose treatment group (Fig. 1E). Lastly, serum inflammatory cytokine assays accentuated the remarkable anti-inflammatory attribute of ursolic acid, evidenced by the marked reduction in pro-inflammatory cytokines (Fig. 1F). Further assessments of gene expression levels of inflammatory cytokines in liver tissues showed that intervention with ursolic acid had the most notable improvement effects on TGF-β, IL-1β, IL-6, IL-17A, and IL-23, manifesting that even low-dose intervention treatment could significantly reduce the levels of all these genes (Supplementary Fig. 1B).

Identification of SPP1 as a direct ursolic acid-binding protein

To further elucidate the therapeutic mechanisms by which ursolic acid addresses NAFLD, we initiated our investigative endeavor by querying the GEO database platform for human transcriptomic microarrays associated with NAFLD. Given the pronounced anti-inflammatory effects of ursolic acid, our exploration was sharply focused on immune inflammation, a pivotal juncture in the progression

 https://doi.org/10.3350/cmh.2024.0047

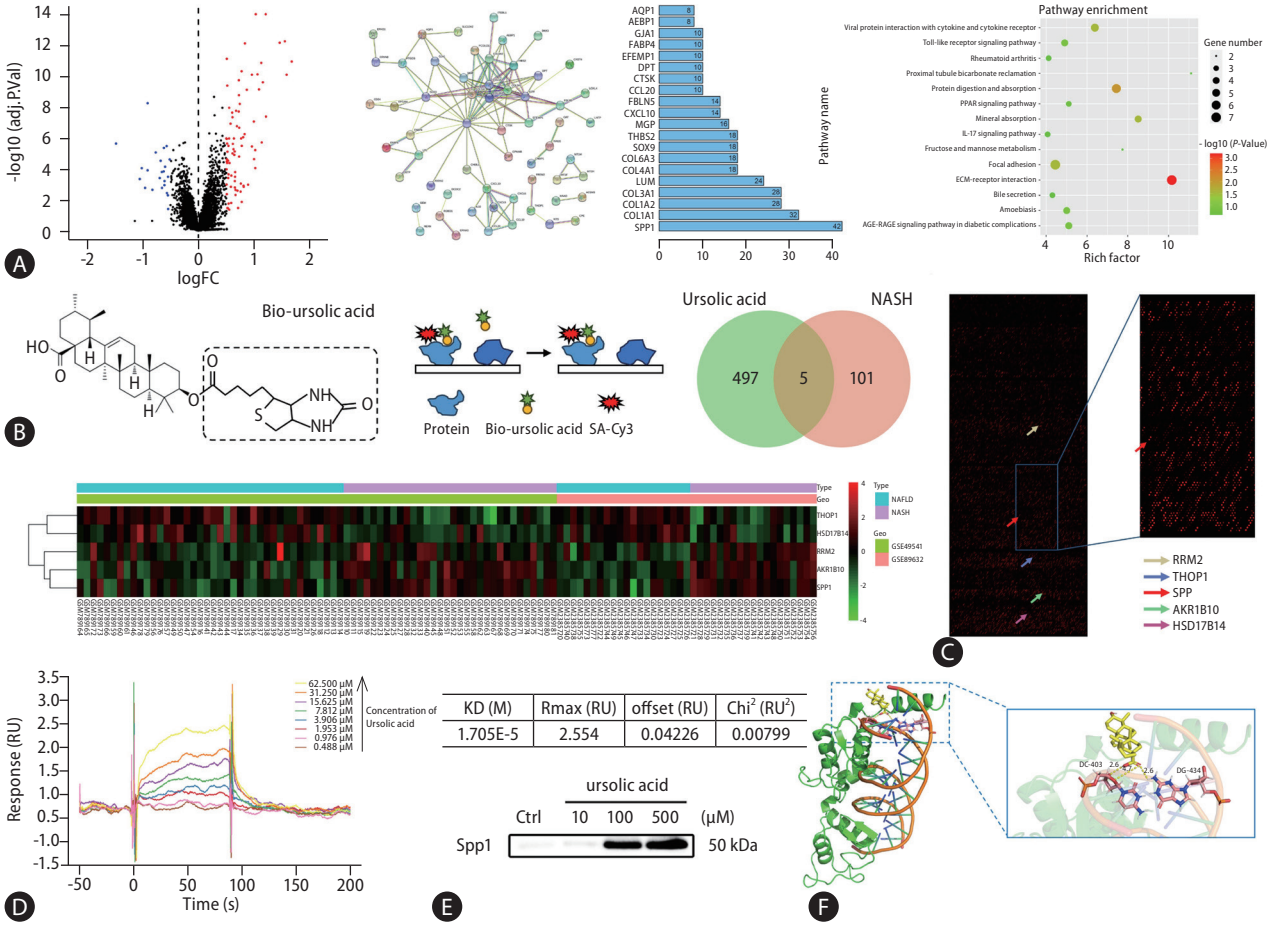

Figure 2. Identification of SPP1 as a direct ursolic acid-binding protein. (A) Bioinformatic analysis was conducted in this study, 106 DEGs were identified from two microarrays, which notably delineated the intricate comparative stages between NAFLD and NASH, and a volcano plot was plotted. A PPI network was constructed for these DEGs using the STRING database, providing insights into the functional relationships between identified proteins. And centrality analysis, pivotal for discerning nodes of paramount importance within the network, was systematically executed based on the intricate interaction relationships between nodes. A pathway enrichment was performed to acquire a holistic understanding of the biological functions and pathways associated with the DEGs. (B) A schematic diagram showed that biotin-labeled ursolic acid was co-incubated with this array, followed by signal interpretation using Cy3-streptavidin. (C) 502 targets were identified that interacted directly with ursolic acid, and intersection analysis with the previously identified DEGs retained five candidates, wherein the differentially binding proteins were presented in the proteomics chip and heatmap. (D) The SPR analysis was produced using a biacore sensor chip, wherein the molecular dynamics analysis revealed that ursolic acid and SPP1 exhibited high-affinity interaction, with the equilibrium dissociation constant of 1.705E-5. (E) A pull-down assay was performed to further verify the binding affinity between ursolic acid and SPP1 in vivo. (F) The molecular docking simulation showed a mutual binding between ursolic acid and SPP1, with a binding energy of –5.8. SPP1, secreted phosphoprotein 1; DEGs, differentially expressed genes; NAFLD, nonalcoholic fatty liver disease; NASH, nonalcoholic steatohepatitis; STRING, Search Tool for the Retrieval of Interacting Genes; SPR, surface plasmon resonance; KD, knockdown.

from NAFLD to NASH.[22] Consequently, two microarrays, specifically GSE49541 and GSE89632, were incorporated, which distinctly delineated the comparative stages between NAFLD and NASH, encompassing 40 and 20 samples of NAFLD, as well as 32 and 19 samples of NASH, respectively (Supplementary Fig. 2). After batch normalization, 106 differentially expressed genes (DEGs) were identified, and a PPI network was constructed for all of them, while centrality analysis disclosed that SPP1 occupied the highest weight within this framework (Fig. 2A and Supplementary Table 2). Enrichment analysis underscored the ECM-receptor interaction pathway as the most differentially enriched. It is noteworthy that numerous studies have asserted the ECM components, apart from serv-

https://doi.org/10.3350/cmh.2024.0047

ing as a structural scaffold, can also facilitate intercellular communication as signaling mediators and plays a crucial role in the progression of NAFLD, especially in inflammation and fibrosis processes, with SPP1 as an integral component.[16]

Simultaneously, the HuProt™20K human proteome microarray was employed for high-throughput screening of direct protein targets of ursolic acid. During this procedure, biotin-labelled ursolic acid was co-incubated with this array, followed by signal interpretation using Cy3-streptavidin, revealing 502 potential targets that interacted directly with ursolic acid, while intersection analysis with the previously identified DEGs retained five candidates: SPP1, PRM2, THOP1, HSD17B14 and AKR1B10 (Fig. 2B, C and Supplementary Table 3). Receiver operating characteristic curves, generated from the transcriptomic chip data, were plotted to assess the sensitivity and specificity between these candidates and NAFLD progression, and the results showed that the area under the curve values for all five genes exceeded 0.75, indicating their substantial relevance (Supplementary Fig. 3A).

Next, biomolecular interaction analyses were executed based on Surface Plasmon Resonance (SPR) technology to ascertain the binding affinity of these five proteins with ursolic acid. Surprisingly, PRM2, THOP1 and AKR1B10 manifested no detectable binding with ursolic acid, leaving only SPP1 and HSD17B14 to exhibit high-affinity interactions, with equilibrium dissociation constants of 1.705E-5 and 7.329E-6, respectively (Fig. 2D and Supplementary Fig. 3B). Relevant studies on HSD17B14 accentuated its role in the NAD-dependent conversion of estradiol to estrone, suggesting it might be implicated in modulating lipid and sterol metabolism in the pathophysiology of NAFLD.[23] However, considering our focal point on immune inflammation, and the paramount significance SPP1 might hold in the shift from NAFLD to NASH, our subsequent experiments centred on SPP1, while sidelining HSD17B14. To further authenticate the physiological interaction between ursolic acid and SPP1, a pull-down assay was conducted by co-incubating various concentrations of ursolic acid with murine liver tissue lysates. SPP1 protein expression was detected in the precipitates, indicating mutual binding between ursolic acid and SPP1 in vivo (Fig. 2E). Furthermore, ELISA assay was used to evaluate the SPP1 expression within the ECM. During this process, liver tissues were dissociated and filtered to exclude the interference from intracellular protein components, and the results suggested that ursolic acid could operate in the extracellular regions by capturing secreted SPP1 (Supplementary Fig. 3C). Additionally, the in silico molecular docking simulation projected a binding energy of −5.8 between ursolic acid and SPP1, consistent with our prior experimental outcomes of their strong affinity (Fig. 2F).

SPP1 gene knockdown affords protective effects against HFD-induced MASLD

Moving forward, it is imperative to experimentally substantiate the pivotal role of SPP1 in the progression of MASLD. To circumvent the potential perturbations of embryonic and developmental gene knockdown (KD) on the intrinsic metabolic and inflammatory phenotypes, adeno-associated virus (AAV) was employed to establish an SPP1 KD model in mature mice. Besides, considering that SPP1 is concurrently expressed by resident immune cells, parenchymal cells, and recruited blood-derived inflammatory cells, liver-specific promoters like TBG were bypassed in favor of the broad-spectrum CMV promoter. Thus, we opted for the serotype AAV2/8 to deliver CMV-driven shSPP1 into wild-type mice (Fig. 3A). While mice injected with the empty virus AAV2/8-CMV-Null were maintained as wild-type controls (WT). Ultimately, successful knockdown was affirmed by the marked reduction in SPP1 protein expression in the liver tissues derived from these KD mice.

Animal studies subsequently revealed that SPP1 KD conferred a degree of protection against HFD-induced weight gain in mice. Interestingly, this weight differential emerged from the ninth week, a time point posterior to the intervention by ursolic acid, and the magnitude of weight reduction was considerably milder. Given that HFD-induced mice were known to exhibit hepatic chronic inflammatory responses between the sixth to eighth weeks,[24] while recognizing the intertwined relationship between chronic inflammation and hepatic metabolic processes,[25] we postulated that the weight reduction ascribed to SPP1 KD stems from its anti-inflammatory effects (Fig. 3B). Multiple metrics, encompassing liver weights, liver indexes, as well as serum and hepatic triglyceride and total cholesterol levels consistently evinced that SPP1 KD could ameliorate hepatic lipid accumulation in high-fat diet-fed mice to some

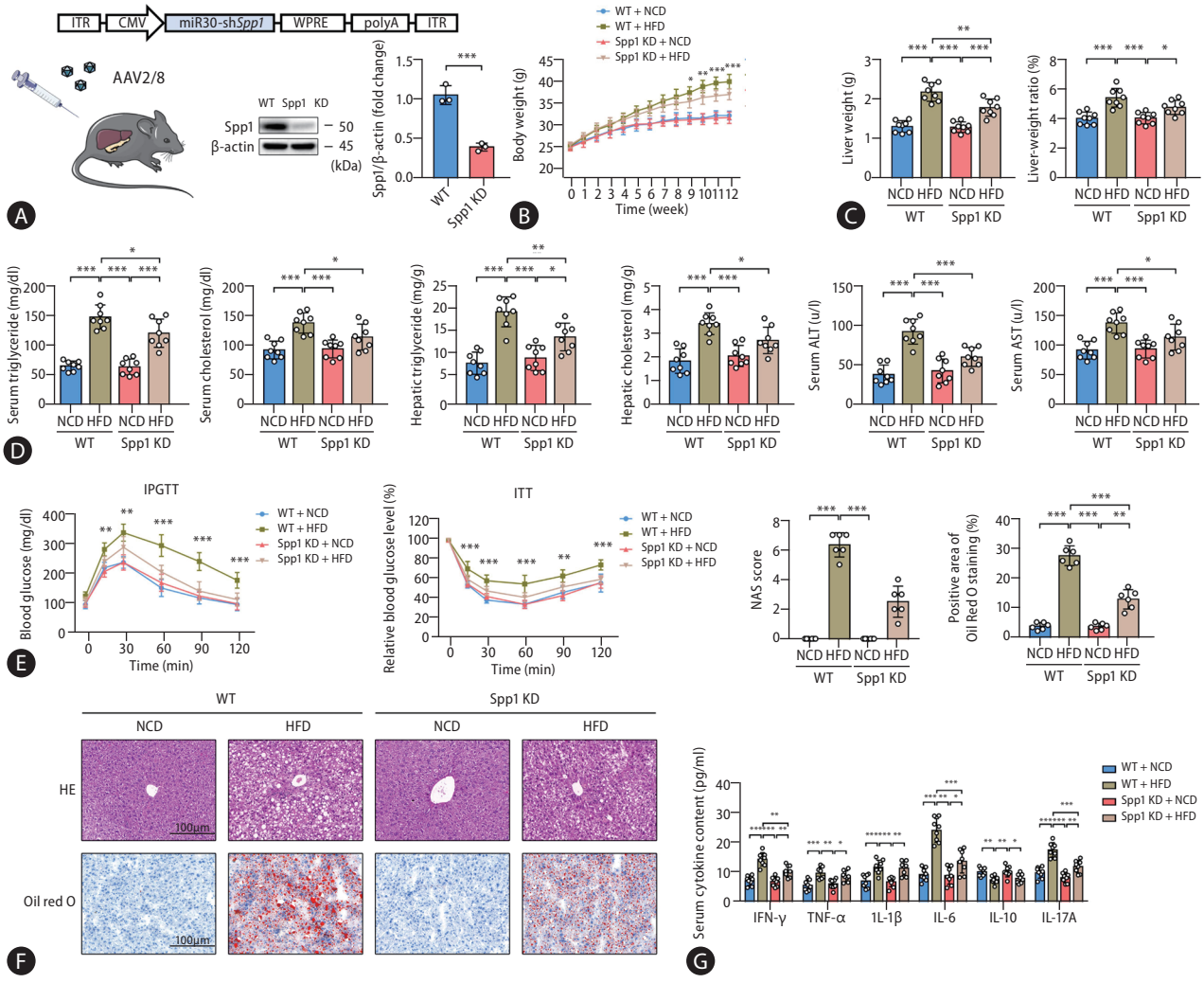

Figure 3. SPP1 gene knockdown affords protective effects against HFD-induced MASLD. (A) Schematic diagram revealed the protocol of SPP1 knockdown. Specifically, AAV2/8 vectors harboring a CMV-driven shRNA targeting SPP1 were employed for in vivo gene delivery. Western blot analyses demonstrated a marked reduction in SPP1 protein expression in the liver tissues from these KD mice, thus affirming the successful knockdown. Subsequently, mice were fed with HFD to construct the MASLD mice model. (B) Body weights were recorded weekly. (C) Liver weights were measured by the termination of this experiment at the twelfth week, and liver indexes were calculated by the ratio of liver to body weight. (D) Serum and hepatic lipid concentrations were determined by an automatic biochemical analyzer. (E) IPGTT and ITT were performed to monitor glucose tolerance and insulin resistance. (F) Histological staining of H&E and oil red O in liver tissues was performed to observe the inflammatory cytokine infiltration and lipid droplet accumulation. (G) Serum inflammatory cytokines were determined to detect inflammatory reactions. SPP1, secreted phosphoprotein 1; HFD, high-fat diets; MASLD, metabolic dysfunction-associated steatotic liver disease; AAV, adeno-associated virus; KD, knockdown; IPGTT, intraperitoneal glucose tolerance tests; ITT, insulin tolerance tests; SD, standard deviation. Data are represented as mean±SD. n=3-8. *P<0.05, **P<0.01, ***P<0.001.

extent, albeit less efficacious than ursolic acid intervention, aligning with our supposition (Fig. 3C). Furthermore, while mitigating HFD-induced liver inflammation and steatosis effectively, SPP1 KD concomitantly conferred robust protection against hepatic functional impairment and insulin resistance, which might be attributed to the alleviation of immune inflammation, a linchpin in the evolution of MASLD, thereby ameliorating associated oxidative stress, autophagy and apoptosis (Fig. 3E, F, and Supplementary Fig. 4A). Reinforcing our prior evaluations, subsequent analyses of inflammatory cytokines in both serum and hepatic tissues invariably spotlighted that SPP1 KD could substantially suppress the expression levels of IFN-γ, TGF-β, IL-6, IL-17A, IL-21 and IL-23, hinting at a potential

https://doi.org/10.3350/cmh.2024.0047

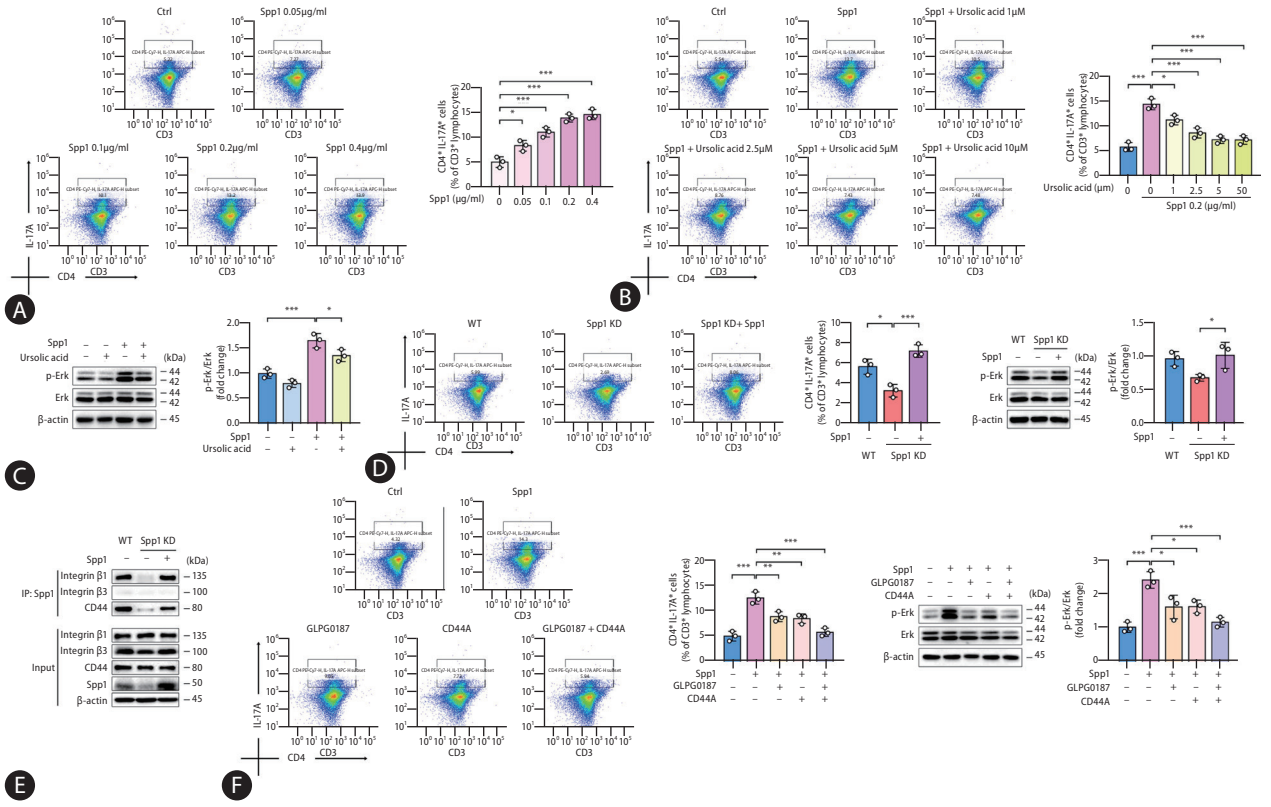

Figure 4. SPP1 promotes Th17 cell differentiation via interactions with ITGB1 and CD44. (A) Flow cytometry revealed a dose-dependent facilitation of Th17 differentiation by SPP1, with a concentration of 0.2 μg/mL emerging as optimal for ensuing experimental endeavors. Th17 cells were identified as $CD3^+CD4^+IL\text{-}17A^+$ cells, and these results were represented as the percentage of Th17 cells among $CD3^+$ T cells. (B) Flow cytometry indicated that ursolic acid dose-dependently inhibited SPP1-induced Th17 cell differentiation, with a concentration of 5 μM emerging as optimal for subsequent investigative pursuits. (C) Western blot analyses were conducted to detect the phosphorylation level of ERK protein. (D) SPP1 KD decreased the ERK phosphorylation level and substantially curtailed Th17 cell differentiation. (E) Co-immunoprecipitation analyses suggested strong interactions between SPP1 and both ITGB1 and CD44. (F) Both ITGB inhibitors and CD44 antagonists suppressed the SPP1-driven Th17 cell differentiation, with an even more pronounced inhibitory effect upon their combined application. SPP1, secreted phosphoprotein 1; ITGB1, integrin β1; CD44A, CD44 antagonists; ERK, extracellular signal-regulated kinase; SD, standard deviation. Data are represented as mean±SD. n=3. *P<0.05, **P<0.01, ***P<0.001.

mechanistic nexus with Th17 cells (Fig. 3G and Supplementary Fig. 4B).

SPP1 promotes Th17 cell differentiation via interactions with ITGB1 and CD44

Diving into the molecular intricacies, our exploration probed the possibility of SPP1 driving Th17 cell differentiation as a therapeutic target for ursolic acid. Isolated primary $CD4^+$ T cells were harvested from healthy murine spleens and subjected to a precise set of stimulatory conditions. During this process, recombinant SPP1 proteins at varying concentrations were integrated into the culture medium to foster the differentiation of Th17 cells, and flow cytometry analyses subsequently affirmed that SPP1 could dose-dependently potentiate Th17 cell differentiation, stabilizing its stimulatory prowess at a concentration of 0.2 μg/mL, which was selected for ensuing experimental endeavors (Fig. 4A). In parallel, when exposed to diverse concentrations of ursolic acid in the presence of recombinant SPP1, it was apparent that ursolic acid exerted a dose-dependent inhibition on the SPP1-induced Th17 cell differentiation, with a concentration of 5 μM emerging as optimal for subsequent investigative pursuits (Fig. 4B).

Typically, the canonical pathway attributed to SPP1-induced Th17 cell differentiation hinges on the activation of CD44 receptors on antigen-presenting cells, such as macrophages and dendritic cells.[18] This engagement triggers

alterations in the domain of major histocompatibility complex, facilitating the interaction with initial CD4$^+$ T cells, thus triggering a cascade of cytokine releases including TGF-β and IL-6 that ultimately activates Th17 cells.[26] However, recent investigations allude to the existence of an alternate IL-6/STAT3-independent pathway wherein SPP1 propels Th17 cell differentiation.[27,28] Considering SPP1's intrinsic propensity as an adhesive protein to interact with an array of cell surface receptors like integrins and CD44, our study aimed to co-incubate cells, either exposed to or spared from SPP1 and ursolic acid stimuli, with recombinant SPP1, followed by Co-immunoprecipitation (Co-IP) analyses. The precipitates were probed for the protein expressions of ITGB1, ITGB3 and CD44, inspired by interaction data retrieved from online databases suggesting their putative interactions between SPP1 and integrins at the αvβ1 and αvβ3 junctures.[29] Intriguingly, ITGB1 and CD44 protein expressions were ubiquitously detected in all cellular precipitates, with cells co-treated with ursolic acid exhibiting conspicuous reductions in these protein levels, suggesting a physiological interaction between SPP1 and both ITGB1 and CD44 within cells, which is susceptible to modulation by ursolic acid (Supplementary Fig. 5). However, ITGB3 displayed conspicuously absent across all samples counterintuitively, hinting at a potential weak affinity between SPP1 and ITGB3, precluding the formation of stable com-

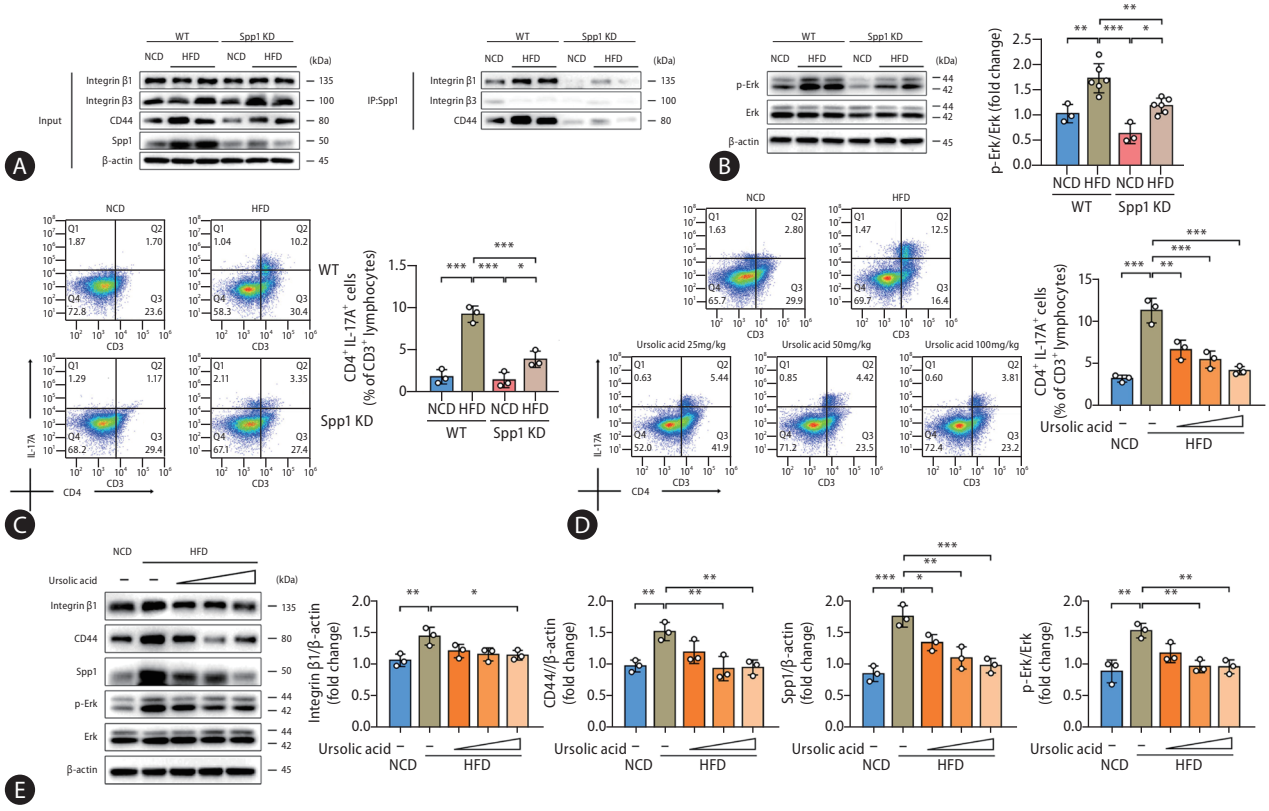

Figure 5. Ursolic acid modulates SPP1-mediated Th17 cell differentiation to ameliorate MASLD. (A–C) Mice were derived from the experiments of SPP1 KD, wherein (A) presented that the protein levels of ITGB1 and CD44 expressed in the pull-down products were conspicuously surged by HFD administration, whereas a precipitous decline in their expression was observed in the liver tissue lysates procured from the SPP1 KD mice, while (B) demonstrated that such alterations were concomitant with trends in the phosphorylation level of ERK protein; and concurrently, (C) displayed a similar trend in hepatic Th17 cell populations. (D, E) Mice were derived from the first part of experiments, those were fed with HFD and different concentrations of ursolic acid, wherein (D) suggested that ursolic acid dose-dependently ameliorated the escalated Th17 cell populations induced by the high-fat dietary regimen, and (E) revealed consistent protein levels of SPP1, ITGB1, CD44, as well as the phosphorylation level of ERK. Data are represented as mean±SD. n=3-6. *P<0.05, **P<0.01, ***P<0.001. SPP1, secreted phosphoprotein 1; MASLD, metabolic dysfunction-associated steatotic liver disease; KD, knockdown; ITGB1, integrin β1; CD44A, CD44 antagonists; HFD, high-fat diets; ERK, extracellular signal-regulated kinase; SD, standard deviation.

https://doi.org/10.3350/cmh.2024.0047

plexes that could be precipitated. Since activated CD44 receptors on the surface of T cells could modulate the phosphorylation modification process of ERK via the serine/threonine protein kinase Raf-1, while the protein complex formed by SPP1 and ITGB1 could similarly regulate the ERK signaling pathway through AKT (i.e., Rac), eventually enhancing the transcription level of retinoic acid-related orphan receptor (ROR) gamma, we gauged the protein expression of their common downstream, ERK.[29-31] Western blot analyses illuminated that the intervention of SPP1 significantly upregulated the phosphorylation level of ERK, whereas this effect was adeptly counteracted by ursolic acid (Fig. 4C).

To bolster our understanding of the SPP1-facilitated mechanism underlying Th17 cell differentiation, the SPP1 KD mice were revisited, isolating splenic $CD4^+$ T cells therefrom. The empirical findings demonstrated a distinct diminution in Th17 cell differentiation in the wake of SPP1 KD, a phenomenon that the reintroduction of recombinant SPP1 could resurrect, with ERK phosphorylation patterns echoing this trend (Fig. 4D). Subsequent immunoprecipitation assays unveiled that ITGB1 and CD44 expressions were conspicuously absent in precipitates from SPP1 KD-derived cells, and their expressions were rejuvenated upon supplementation with the recombinant protein, reasserting the physiological binding of SPP1 with ITGB1 and CD44 (Fig. 4E). Finally, leveraging $CD4^+$ T cells from healthy murine spleens, and concurrently administering recombinant SPP1 with either ITGB inhibitors (i.e., GLPG0187) or CD44 antagonists (CD44A), our results manifested that both ITGB and CD44 were instrumental in mediating the SPP1-driven Th17 cell differentiation, with an even pronounced inhibitory effect upon their combined application, which pointed towards the convergence of their downstream signaling through the ERK pathway (Fig. 4F).

Ursolic acid modulates SPP1-mediated Th17 cell differentiation to ameliorate MASLD

Drawing upon our preliminary experimental findings, in vivo studies were instigated to corroborate these observations. Remarkably, immunoprecipitation analyses showed that both ITGB1 and CD44 were ubiquitously expressed in the pull-down products from liver tissues of WT mice, with their expression surging conspicuously in the context of HFD administration (Fig. 5A). Conversely, a precipitous decline in their expression was observed in the liver tissue lysates procured from the SPP1 KD mice, while such alterations were concomitant with trends in the phosphorylation level of ERK protein (Fig. 5B). Flow cytometry analyses displayed an upsurge in hepatic Th17 cell populations in high-fat diet-fed mice, an anomaly rectified by SPP1 KD, and immunohistochemical staining of liver tissues for SPP1, ROR gamma, and IL-17A presented consistent results, which were also confirmed by assessments of gene expression (Fig. 5C, Supplementary Fig. 1B, and Supplementary Fig. 6A).

Lastly, our research circled back to the therapeutic potential of ursolic acid. Both flow cytometry and immunohistochemical staining unanimously demonstrated that ursolic acid could dose-dependently ameliorate the escalated Th17 cell populations in the liver tissues of mice induced by the high-fat dietary regimen (Fig. 5D, Supplementary Fig. 4B, and Supplementary Fig. 6B). Additionally, Western blot analyses illuminated that the intervention of ursolic acid conspicuously reduced the protein levels of SPP1, ITGB1 and CD44, alongside restraining the phosphorylation status of ERK in mouse liver tissues (Fig. 5E).

Taken together, all these findings validated our experimental hypothesis that ursolic acid could ameliorate the immune inflammation in MASLD by modulating SPP1-mediated Th17 cell differentiation, with the ERK signaling pathway, orchestrated jointly by ITGB1 and CD44, emerging as a linchpin in this molecular cascade.

DISCUSSION

In the current global health landscape, MASLD has emerged as the most prevalent chronic liver condition, with epidemiological surveys compellingly indicating that over 170 million adults worldwide are grappling with its ramifications, leading to an alarming synchronic uptick in liver transplantations, hepatocellular carcinomas, and liver-associated mortalities.[5,32] Alongside, the metabolically intertwined nature of MASLD with disorders such as obesity, type 2 diabetes, and hyperlipidemia, paints a daunting picture of its economic impact on global health infrastructure, that direct medical expenses related to MASLD in the United States alone have exceeded $100 billion by estimate.[2,33]

A troubling trend is the downward shift in the age demographic of those affected, implying that an increasing number of individuals might suffer prolonged exposure to MASLD and its associated complications, exacerbating the strain on the global health milieu.[34,35] As such, a consensus statement, crafted by a multidisciplinary consortium of global experts in 2022, has categorically designated MASLD as a chronic metabolic public health malady, underscoring its prominence in the global health quandaries whilst amplifying the dire need to address such metabolic ailments.[36]

While the pathophysiological intricacies of MASLD, involving a labyrinthine interplay of myriad cellular entities and signaling cascades, remain not entirely deciphered, burgeoning evidence points toward metabolic disruption and immune inflammation as core players.[37] Recent international expert consensuses have reconceptualized MASLD, emphasizing metabolic dysfunctions with the terms metabolic dysfunction-associated fatty liver disease (MAFLD) and metabolic dysfunction-associated steatotic liver disease (MASLD).[38,39] Within these consensus frameworks, the term steatohepatitis is felt to be an important pathophysiological concept that should be retained, while immune inflammation is pinpointed as the crux in the progression of MASLD.

A plethora of studies denote that Th17 cell-mediated immune-inflammatory responses, acting as cardinal modulators of immune stress and inflammation, are intrinsically intertwined with every juncture of MASLD evolution.[37] In the milieu of MASLD-afflicted hepatic tissues, a persistently chronic low-grade inflammation fosters an immunological microenvironment wherein various cytokines, inclusive of TGF-β and IL-6, experience surges.[10] These cytokines synergistically propel Th17 cell differentiation, thus culminating in copious IL-17 production.[13] Notably, IL-17 is a potent inflammatory mediator capable of instigating hepatocytes to unleash a plethora of chemokines, hence recruiting an even greater pool of immune cells into the liver, amplifying the inflammatory cascade.[40] Concurrently, IL-17 wields influence, either directly or indirectly, over HSCs, promoting their proliferation and collagen synthesis, thereby hastening the fibrotic trajectory.[41,42] Integral to this process, the ECM, a fundamental architectural component of tissue structures, not only furnishes cellular stability but is also replete with fibronectins, adhesion proteins, polysaccharides, proteases and growth factors, underpinning cellular dialogues.[43] Given this backdrop, therapeutic strategies targeting the ECM components and Th17 cells have proffered novel therapeutic avenues for MASLD, encompassing matrix metalloproteinase inhibitors, transforming growth factor-β inhibitors and CXC chemokine receptor antagonists.[44] While these pharmacological agents have evinced promise in attenuating inflammation and fibrosis, they remain in the nascent stages of clinical trials, awaiting widespread validation and deployment.[6]

Ursolic acid, a natural compound endowed with an extensive array of biological activities, has garnered considerable attention in the realm of biomedical research in recent years.[7] When employed as a prophylactic or therapeutic agent for MASLD, ursolic acid primarily augments hepatic lipid metabolic capacities, which is achieved by activating intracellular signaling pathways such as AMPK and PPARα thereby fostering the β-oxidation of fatty acids whilst concurrently curtailing their synthesis.[45] In parallel, this compound has been empirically demonstrated to possess pronounced antiinflammatory and antioxidative attributes, as it modulates a suite of signaling molecules intricately intertwined with oxidative stress and inflammatory cascades, including but not limited to Nrf2, HO-1 and NF-κB.[46,47] Additionally, ursolic acid thwarts the progression of hepatic fibrosis and decelerates the transition from MASLD to MASH by suppressing the TGF-β/Smad signaling pathway, which in turn curbs the activation of HSCs and the accumulation of ECM components.[48]

Our previous researches have elucidated that ursolic acid exhibits dual protective capacities by modulating IGF-IR and HIF-1 signaling pathways, offering fortification against metabolic dysfunction and hepatic hypoxia.[21] In this present investigation, we further discerned that ursolic acid could also hinder the protein activity of SPP1 within the ECM, subsequently attenuating the activation state of Th17 cells and modulating cytokine-mediated intercellular crosstalk, ameliorating immunological cascade reactions during MASLD evolution. A seminal discovery of this study is the elucidation of the mechanism whereby SPP1, beyond its traditional TGF-β/IL-6 cytokine pathway, can directly engage with ITGB1 and CD44, modulating their joint downstream ERK signaling pathway and thereby inducing Th17 cell differentiation - a molecular mechanism paramount to ursolic acid's regulation of SPP1 and its subsequent allevi-

https://doi.org/10.3350/cmh.2024.0047

ation of immune inflammation. Excitingly, emerging discourse has pinpointed that exercise, a pivotal lifestyle intervention strategy for metabolic disorders, may confer systemic metabolic benefits triggered in both muscles and non-contractile tissues, and its operative mechanism could be intimately linked to ITGB1, underscoring the significance of this integrin as a potential epicentre of metabolic inflammatory responses that warrant meticulous scrutiny.[49] Hence, a profound understanding of its underlying mechanisms might pave the way for innovative therapeutic strategies, heralding renewed hope for MASLD patients.

Limitations should be acknowledged in this exploration. As the molecular target central to our investigation, SPP1 exists two discrete isoforms: the secreted one and the intracellular one, with our emphasis predominantly casting on the former, an integral component of the ECM, due to its pivotal role as a secretory factor capable of mediating intercellular communication in metabolic inflammatory reactions;[18,19] in contrast, existing research on the latter posits its pro-inflammatory role chiefly via activation of the intracellular Toll-like receptor signaling pathway, especially the critical MyD88 signal transducer, thus catalysing the secretion of various inflammatory cytokines—a domain beyond the purview of our present endeavour.[26] On another note, a spate of innovative techniques, including single-cell sequencing and DSP spatial multi-omics analysis, have emerged as exceptionally conducive to investigating cytokine-mediated metabolic stress and immune inflammation. Yet, given they were not universally adopted at the onset of our study and hence remained unutilized herein. Nevertheless, our ongoing endeavours encompass sequencing of MASLD samples at various stages, aspiring to unearth the intricate pathophysiological mechanisms underpinning MASLD progression through pseudo-temporal analyses. This, synergized with subsequent foundational and clinical trial investigations, seeks to provide novel insights, revolutionizing prevention and therapeutic strategies, ultimately aiming to enhance the quality of life and prognosis for MASLD patients.

Authors' contribution

YZ, FL, and YL conceived the idea for this work and designed the experiments. YZ, LZ, and ZX performed the whole experiment. CH, QY, DF, YF, SG, CC, JL, YZ and JL contributed the data. All authors read and approved the final manuscript.

Acknowledgements

This work was supported by the National Natural Science Foundation of China (82104549), Natural Science Foundation of Shanghai (3ZR1461200), Shanghai Municipal Health Commission (20234Y0142), China Postdoctoral Science Foundation (2022M722158), Shanghai Medical Innovation & Development Foundation (WL-YXBS-2022001K), and Guangdong Province Traditional Chinese Platform Construction (Key Discipline Hepatology Department).

Conflicts of Interest

The authors have no conflicts to disclose.

SUPPLEMENTARY MATERIAL

Supplementary material is available at Clinical and Molecular Hepatology website (http://www.e-cmh.org).

REFERENCES

1. Wang XJ, Malhi H. Nonalcoholic fatty liver disease. Ann Intern Med 2018;169:ITC65-ITC80.
2. Younossi Z, Anstee QM, Marietti M, Hardy T, Henry L, Eslam M, et al. Global burden of NAFLD and NASH: trends, predictions, risk factors and prevention. Nat Rev Gastroenterol Hepatol 2018;15:11-20.
3. Polyzos SA, Kountouras J, Mantzoros CS. Obesity and nonalcoholic fatty liver disease: From pathophysiology to therapeutics. Metabolism 2019;92:82-97.
4. Simon TG, Roelstraete B, Khalili H, Hagström H, Ludvigsson JF. Mortality in biopsy-confirmed nonalcoholic fatty liver disease: results from a nationwide cohort. Gut 2021;70:1375-1382.
5. Sanyal AJ. Past, present and future perspectives in nonalcoholic fatty liver disease. Nat Rev Gastroenterol Hepatol 2019;16:377-386.
6. Harrison SA, Allen AM, Dubourg J, Noureddin M, Alkhouri N. Challenges and opportunities in NASH drug development. Nat Med 2023;29:562-573.
7. Mlala S, Oyedeji AO, Gondwe M, Oyedeji OO. Ursolic acid and its derivatives as bioactive agents. Molecules 2019;24:2751.

8. Wang Y, Wu J, Shi A. Literature review on the use of herbal extracts in the treatment of non- alcoholic fatty liver disease. Endocr Metab Immune Disord Drug Targets 2022;22:1123-1145.
9. Gong P, Long H, Guo Y, Wang Z, Yao W, Wang J, et al. Chinese herbal medicines: The modulator of nonalcoholic fatty liver disease targeting oxidative stress. J Ethnopharmacol 2024;318:116927.
10. Friedman SL, Neuschwander-Tetri BA, Rinella M, Sanyal AJ. Mechanisms of NAFLD development and therapeutic strategies. Nat Med 2018;24:908-922.
11. He B, Wu L, Xie W, Shao Y, Jiang J, Zhao Z, et al. The imbalance of Th17/Treg cells is involved in the progression of nonalcoholic fatty liver disease in mice. BMC Immunol 2017;18:33.
12. Van Herck MA, Weyler J, Kwanten WJ, Dirinck EL, De Winter BY, Francque SM, et al. The differential roles of T cells in non-alcoholic fatty liver disease and obesity. Front Immunol 2019;10:82.
13. Gomes AL, Teijeiro A, Burén S, Tummala KS, Yilmaz M, Waisman A, et al. Metabolic inflammation-associated IL-17A causes non-alcoholic steatohepatitis and hepatocellular carcinoma. Cancer Cell 2016;30:161-175.
14. Sun G, Zhao X, Li M, Zhang C, Jin H, Li C, et al. CD4 derived double negative T cells prevent the development and progression of nonalcoholic steatohepatitis. Nat Commun 2021;12:650.
15. Zhou Y, Zhang H, Yao Y, Zhang X, Guan Y, Zheng F. CD4+ T cell activation and inflammation in NASH-related fibrosis. Front Immunol 2022;13:967410.
16. Shim YR, Jeong WI. Recent advances of sterile inflammation and inter-organ cross-talk in alcoholic liver disease. Exp Mol Med 2020;52:772-780.
17. Moreno-Fernandez ME, Giles DA, Oates JR, Chan CC, Damen MSMA, Doll JR, et al. PKM2-dependent metabolic skewing of hepatic Th17 cells regulates pathogenesis of nonalcoholic fatty liver disease. Cell Metab 2021;33:1187-1204.e9.
18. Uede T. Osteopontin, intrinsic tissue regulator of intractable inflammatory diseases. Pathol Int 2011;61:265-280.
19. Song Z, Chen W, Athavale D, Ge X, Desert R, Das S, et al. Osteopontin takes center stage in chronic liver disease. Hepatology 2021;73:1594-1608.
20. Li Y, Xiu W, Xu J, Chen X, Wang G, Duan J, et al. Increased CHCHD2 expression promotes liver fibrosis in nonalcoholic steatohepatitis via Notch/osteopontin signaling. JCI Insight 2022;7:e162402.
21. Zheng Y, Huang C, Zhao L, Chen Y, Liu F. Regulation of decorin by ursolic acid protects against non-alcoholic steatohepatitis. Biomed Pharmacother 2021;143:112166.
22. Hammerich L, Tacke F. Hepatic inflammatory responses in liver fibrosis. Nat Rev Gastroenterol Hepatol 2023;20:633-646.
23. Gao S, Zhao J, Xu Q, Guo Y, Liu M, Zhang C, et al. MiR-31 targets HSD17B14 and FSHR, and miR-20b targets HSD17B14 to affect apoptosis and steroid hormone metabolism of porcine ovarian granulosa cells. Theriogenology 2022;180:94-102.
24. Kawano Y, Nakae J, Watanabe N, Kikuchi T, Tateya S, Tamori Y, et al. Colonic pro-inflammatory macrophages cause insulin resistance in an intestinal Ccl2/Ccr2-dependent manner. Cell Metab 2016;24:295-310.
25. Zhao P, Wong KI, Sun X, Reilly SM, Uhm M, Liao Z, et al. TBK1 at the crossroads of inflammation and energy homeostasis in adipose tissue. Cell 2018;172:731-743.e12.
26. Rittling SR, Singh R. Osteopontin in immune-mediated diseases. J Dent Res 2015;94:1638-1645.
27. Yan A, Luo G, Zhou Z, Hang W, Qin D. Tear osteopontin level and its relationship with local Th1/Th2/Th17/Treg cytokines in children with allergic conjunctivitis. Allergol Immunopathol (Madr) 2018;46:144-148.
28. Liu W, Zeng Q, Zhou L, Li Y, Chen Y, Luo R. Leptin/osteopontin axis contributes to enhanced T helper 17 type responses in allergic rhinitis. Pediatr Allergy Immunol 2018;29:622-629.
29. Zeng B, Zhou M, Wu H, Xiong Z. SPP1 promotes ovarian cancer progression via Integrin β1/FAK/AKT signaling pathway. Onco Targets Ther 2018;11:1333-1343.
30. Wang JB, Zhang Z, Li JN, Yang T, Du S, Cao RJ, et al. SPP1 promotes Schwann cell proliferation and survival through PKCα by binding with CD44 and αvβ3 after peripheral nerve injury. Cell Biosci 2020;10:98.
31. Lee HC, Liu FC, Tsai CN, Chou AH, Liao CC, Yu HP. Esculetin ameliorates lipopolysaccharide-induced acute lung injury in mice via modulation of the AKT/ERK/NF-κB and RORγt/IL-17 pathways. Inflammation 2020;43:962-974.
32. Anstee QM, Reeves HL, Kotsiliti E, Govaere O, Heikenwalder M. From NASH to HCC: current concepts and future challenges. Nat Rev Gastroenterol Hepatol 2019;16:411-428.
33. Huang DQ, El-Serag HB, Loomba R. Global epidemiology of NAFLD-related HCC: trends, predictions, risk factors and prevention. Nat Rev Gastroenterol Hepatol 2021;18:223-238.
34. Mann JP, Valenti L, Scorletti E, Byrne CD, Nobili V. Nonalcoholic fatty liver disease in children. Semin Liver Dis 2018;38:1-13.

35. Selvaraj EA, Mózes FE, Jayaswal ANA, Zafarmand MH, Vali Y, Lee JA, et al. Diagnostic accuracy of elastography and magnetic resonance imaging in patients with NAFLD: A systematic review and meta-analysis. J Hepatol 2021;75:770-785.
36. Lazarus JV, Mark HE, Anstee QM, Arab JP, Batterham RL, Castera L, et al. Advancing the global public health agenda for NAFLD: a consensus statement. Nat Rev Gastroenterol Hepatol 2022;19:60-78.
37. Huby T, Gautier EL. Immune cell-mediated features of non-alcoholic steatohepatitis. Nat Rev Immunol 2022;22:429-443.
38. Eslam M, Newsome PN, Sarin SK, Anstee QM, Targher G, Romero-Gomez M, et al. A new definition for metabolic dysfunction-associated fatty liver disease: An international expert consensus statement. J Hepatol 2020;73:202-209.
39. Rinella ME, Lazarus JV, Ratziu V, Francque SM, Sanyal AJ, Kanwal F, et al. A multisociety Delphi consensus statement on new fatty liver disease nomenclature. J Hepatol 2023;79:1542-1556.
40. Shen T, Chen X, Li Y, Tang X, Jiang X, Yu C, et al. Interleukin-17A exacerbates high-fat diet-induced hepatic steatosis by inhibiting fatty acid β-oxidation. Biochim Biophys Acta Mol Basis Dis 2017;1863:1510-1518.
41. Giles DA, Moreno-Fernandez ME, Divanovic S. IL-17 Axis driven inflammation in non-alcoholic fatty liver disease progression. Curr Drug Targets 2015;16:1315-1323.
42. Ruiz de Morales JMG, Puig L, Daudén E, Cañete JD, Pablos JL, Martín AO, et al. Critical role of interleukin (IL)-17 in inflammatory and immune disorders: An updated review of the evidence focusing in controversies. Autoimmun Rev 2020;19:102429.
43. Di Donato M, Giovannelli P, Migliaccio A, Castoria G. The nerve growth factor-delivered signals in prostate cancer and its associated microenvironment: when the dialogue replaces the monologue. Cell Biosci 2023;13:60.
44. Yang YY, Xie L, Zhang NP, Zhou D, Liu TT, Wu J. Updates on novel pharmacotherapeutics for the treatment of nonalcoholic steatohepatitis. Acta Pharmacol Sin 2022;43:1180-1190.
45. Cheng J, Liu Y, Liu Y, Liu D, Liu Y, Guo Y, et al. Ursolic acid alleviates lipid accumulation by activating the AMPK signaling pathway in vivo and in vitro. J Food Sci 2020;85:3998-4008.
46. Li JS, Wang WJ, Sun Y, Zhang YH, Zheng L. Ursolic acid inhibits the development of nonalcoholic fatty liver disease by attenuating endoplasmic reticulum stress. Food Funct 2015;6:1643-1651.
47. Tasneem S, Liu B, Li B, Choudhary MI, Wang W. Molecular pharmacology of inflammation: Medicinal plants as anti-inflammatory agents. Pharmacol Res 2019;139:126-140.
48. Yu SS, Chen B, Huang CK, Zhou JJ, Huang X, Wang AJ, et al. Ursolic acid suppresses TGF-β1-induced quiescent HSC activation and transformation by inhibiting NADPH oxidase expression and Hedgehog signaling. Exp Ther Med 2017;14:3577-3582.
49. Kuramoto K, Liang H, Hong JH, He C. Exercise-activated hepatic autophagy via the FN1-α5β1 integrin pathway drives metabolic benefits of exercise. Cell Metab 2023;35:620-632.e5.